A multiparametric CFD analysis of multiphase annular flows for oil and gas drilling applications

A Multiparametric CFD Analysis of Multiphase Annular Flows for Oil and Gas Drilling Applications

Emmanuel I. Epelle and Dimitrios I. Gerogiorgis*

Institute for Materials and Processes (IMP), School of Engineering, University of Edinburgh, The King's Buildings, Edinburgh, EH9 3FB, United Kingdom

**Corresponding author: D.Gerogiorgis@ed.ac.uk (+44 131 6517072)*

ABSTRACT

The increasing global energy demand has pushed the oil industry towards developing more innovative and advanced methods of enhancing oil recovery even under unfavourable technical and environmental conditions. The severity of many operational problems affecting the drilling and production of oil and gas wells is worsened by inaccessibility; hence, remedial efforts must be implemented from afar. One of these problems is ensuring efficient removal of formation rock cuttings with a suitable fluid, whose rheology is often complicated. Furthermore, pressure losses along the annular geometry involved, and decreased Rates of Penetration (ROP) due to accumulated drill cuttings downhole, constitute significant portions of the total energy to be supplied. Thus, the application of sophisticated modelling techniques with credible elucidation of the phase distributions (solids, liquids and gas) and prevalent flow regimes becomes essential, if adequate and economic design of a drilling program is desired. The advent of Computational Fluid Dynamics (CFD) and the growth in the available computational power to support it have provided an unprecedented opportunity to simulate and understand complex real flows, especially when experimental methods become extremely demanding. The present study employs the tool of Computational Fluid Dynamics to simulate a two-phase solid-liquid flow in an annulus based on the analysis of cuttings concentration, pressure drop profiles, axial fluid, and solid velocities as a function of several drilling parameters: drill pipe eccentricity, inclination, drill pipe rotation, ROP and fluid rheology. Special emphasis is however, placed on the impact of changing hole eccentricity on cuttings transport efficiency. The suitability of the Eulerian–Eulerian (EE) multiphase tracking scheme in modelling systems of high volume fractions is fully utilised in this work. A non-Newtonian (power law) fluid model with well-described flow parameters is implemented, considering a uniform cuttings size distribution (3 mm). A commercial CFD software (ANSYS FLUENT^{TM} 17.1) has been used; the descriptive and predictive potential of the CFD software has been confirmed on account of the reasonable agreement with previously published experimental data (a relative error of less than 11% is achieved), as illustrated by the corresponding sensitivity plots. This multi-parametric CFD analysis study of multiphase cutting transport during drilling applications has confirmed that fluid velocity, hole inclination and annular eccentricity are the most influential factors governing the cuttings transport efficiency.

1. Introduction

Increased exploration difficulty has made the petroleum industry modify its classical operational methods and technologies with the target of maximising production at reduced costs (Qutob et al., 2011). Some of these difficulties arise due to the inherent complexity of the environment/location of petroleum resources, increased implementation of deviated hole drilling, and power requirements for effective circulation of drilling fluid in order to ensure continuous removal of drill cuttings. Furthermore, reduced Rates of Penetration (ROP), excessive drill bit wear, stuck drill pipe and re-drilling are some of the problems that arise when a drilling fluid is inappropriately designed to promptly remove drill cuttings (Pereira et al., 2010). Increasing the fluid circulation velocity is one of the most reliable methods the industry has adopted to mitigate these problems; however, the additional pressure that is often generated may cause formation fracture and eventual loss of these expensive drilling fluids into these fractures. Under these circumstances, drilling engineers must monitor and optimise the influence of these significantly intertwined drilling variables in order to achieve reliable and cost-effective design of any drilling program. Cuttings transport phenomena significantly change with respect to other parameters such as varying eccentricities and inclination angles across the entire hole, drill pipe rotation and drill pipe/hole diameter ratio (Ofei et al., 2014).

Computational Fluid Dynamics (CFD) is an efficient modelling technique that allows complex downhole multiphase flow phenomena to be captured in the virtual annular flow geometry (Fig. 1). The application of CFD for the analysis, design and optimisation of drilling programs has often been channelled towards vertical and concentric annular geometries, with few studies focusing on the intricacies that evolve due to hole inclination and eccentric configurations (Li and Kuru, 2003). Another complication characterising the modelling process is the occurrence of multiple phases in the flow domain, which requires robust multiphase closure equations and appropriate fluid-particle tracking models to be incorporated with the principal flow equations, thus enhancing solvability and accurate prediction of the drilling variables of interest (Shankar, 2013).

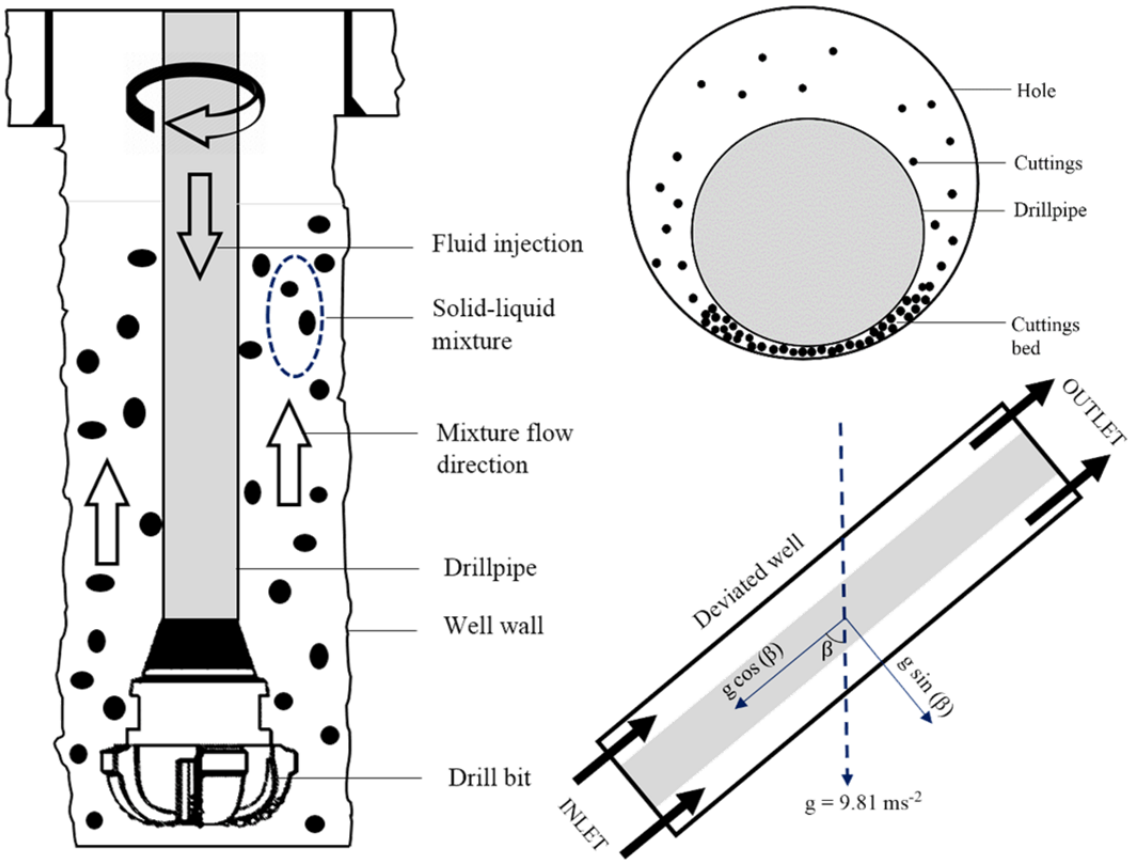

Fig. 1. Hole cleaning during drilling operation with eccentricity and inclination effects.

2. Related Literature

One of the earliest CFD studies conducted to understand cuttings transport phenomena was that of Bilgesu et al. (2002). In their study, the impact of particle size and mud rheology on cuttings removal efficiency was determined using a solid-liquid multiphase flow model. Both water and a non-Newtonian power law fluid were used in horizontal and vertical flow geometries. The results of the simulations showed that annular velocity plays an important role in hole cleaning. In a subsequent study of Bilgesu et al. (2007), steady state CFD simulations were carried out to determine the effects of fluid velocity, cuttings size, drill pipe rotation and inclination angle in deviated wells using the Eulerian model. They observed that the drill pipe rotation aids cuttings removal, especially with smaller particles. CFD studies using foam as the circulating fluid have shown that the power law model performs better than the Herschel-Bulkley model in predicting cuttings transport phenomena. (Rooki et al. 2014; Rooki et al., 2015). The authors examined the effect of foam quality, foam velocity, drill pipe rotation and wellbore inclination on the cuttings transport efficiency and concluded that cuttings removal is enhanced by increasing foam quality and pipe rotation. In their study, the cuttings transport efficiency was examined as a function of the Cuttings Transport Ratio – (CTR, the ratio of annular solids velocity to fluid axial velocity). However, studies conducted by Iyoho et al. 1986, showed that the use of CTR as an index of cuttings removal efficiency could be misleading when particle buildup occurs in inclined or horizontal annuli.

Pereira et al. (2007) studied single-phase non-Newtonian fluid flow in an annulus using CFD techniques. Their study demonstrates the effectiveness of the adopted simulation strategy in replicating experimental data of velocity profiles from literature. Pereira et al. (2010) also analysed multiphase (solid-liquid) flow phenomena in an annulus using the Discrete Phase Model (DPM) with special consideration to particle trajectory as a function of drill pipe rotation. Although their model had good agreements with experimental data, not many drilling variables were considered in their work. Mishra (2007) studied the impact of fluid velocity, cuttings size, ROP, drill pipe rotation and inclination angle on cuttings removal using the Eulerian–mixture model. The findings of Mishra's investigations substantiate the results of Bilgesu et al. (2007) which illustrate that the impact of drill pipe rotation is greater with particles of smaller sizes. It was also shown that fluid flow rate, hole inclination angle and ROP have a major impact on the transport efficiency. Ofei et al. (2014) implemented the Eulerian-Eulerian multiphase model to predict cuttings concentration and pressure losses at different diameter ratios in eccentric horizontal annuli. According to their results, drilling mud had superior transport capabilities compared to water at low diameter ratios; however, the performance of both fluids can be similar at a high diameter ratio of 0.9. Wang et al. (2009) examined cuttings transport in extended reach wells under the influence of drill pipe rotation. Their CFD simulations showed that drill pipe rotation causes an asymmetric deposition of cuttings in the annulus. Sorgun (2010) studied the cuttings transport phenomena using experimental and CFD modelling approaches. It was discovered that drill pipe rotation improves cuttings removal and also decreased the critical fluid velocity required to suspend particles in the flow stream. The work of Yilmaz (2012) involved the development of a CFD model to investigate cuttings bed height and velocities in deviated wellbores using DPM simulations for particle tracking. The one-way Lagrangian-Eulerian (LE) coupling scheme implemented by Yilmaz was found to reasonably represent the transport phenomena of liquid and solid phases, considering the low volume fractions involved. Demiralp (2014) focused on the effects of drill pipe whirling motion on cuttings transport performance in eccentric horizontal annuli. His work featured a two-way coupling of the particle-fluid interactions using the Discrete Element Method (DEM) and consequently discovered a corresponding increase in pressure with an increase in the whirling speed. While much attention has been given to drill pipe rotation by most CFD campaigns, very few research efforts have addressed the impact of changing hole eccentricity along the wellbore, which constitutes a major cause of downhole pressure fluctuations during drilling. We aim to address this challenge. The length of computational domain considered, mesh skewness, orthogonality, and the number of nodes are qualities, which make the developed model more robust, and accurate compared to others. These important properties that determine the quality of solution obtained are not often reported. Section 3.7 describes the improved performance the developed model provides compared to others in literature.

Furthermore, several experimental studies have examined the impact of different drilling variables on the cuttings transport efficiency using both incompressible and compressible drilling

fluids (Han et al., 2010; Osgouei, 2010; Duan et al., 2010; Chen et al., 2007; Iyoho et al., 1986; Capo et al., 2004). The impact of changing hole eccentricity has also not been extensively studied by these experimental methods. Several one–dimensional (across the wellbore) and two-dimensional (across cross-sectional flow area) numerical studies on cuttings transport with a variety of drilling fluids have been conducted (Guckes, 1975; Nguyen and Rahman, 1996; Ozbayoglu et al., 2005; Osunde and Kuru, 2006; Zaisha et al., 2012). However, the use of CFD provides an unparalleled opportunity of analysing multiphase flows in three dimensions. In the present study, cuttings transport phenomena in different annular configurations is investigated using Computational Fluid Dynamics, based on the analysis of cuttings concentration, pressure drop profiles, axial fluid and solid velocities as a function of several drilling parameters: hole eccentricity, inclination, ROP, circulation velocity and fluid rheology. A non-Newtonian fluid (power law) with clearly-defined flow parameters and spherical cuttings of 3 mm diameter are used in the commercial CFD software, (ANSYS FLUENT™ 17.1). A summary of the flow models and closure correlations is presented next, followed by a description of the fluid rheology and annular flow geometry. Subsequently, a mesh independence study is illustrated, after which the results of the model validation against different experimental data is analyzed. Finally, a systematic variation of drilling variables during annular flow is carried out and their impacts on cuttings concentration, pressure drop and axial cuttings velocity are discussed extensively.

3. Methodology

The choice of a multiphase flow-tracking model significantly depends on the governing particle driving force during flow (drag, lift or collision). Nonlinearity of these multiphase interactions yields a variety of flow phenomena, which are modelled using two major approaches: the Lagrangian tracking of computational particles coupled with the Eulerian flow description of the continuous phase and the Eulerian-Eulerian description in which the solid particles are represented as a random field in the Eulerian reference frame (Shankar, 2013). The accuracy of mathematical representation, consistency of accompanying closure models and numerical stability are the attributes that make these techniques very applicable. However, the limitation of the Lagrangian-Eulerian (DPM) approach in handling flow systems involving high solids concentration (>12%) makes the Eulerian-Eulerian approach more suitable for the present study. The Eulerian model describes multiphase flows as interpenetrating continua and incorporates the concept of phasic volume fractions represented as α_q. The annular space occupied by each phase is termed the volume fraction, and conservation laws of mass and momentum are respectively satisfied by each phase (Fluent, 2017). The volume fraction of phase q, V_q is given by:

$$V_q = \int_V \alpha_q dV \tag{1}$$

where

$$\sum_{q=1}^{n} \alpha_q = 1 \tag{2}$$

The effective density of phase 'q' can be written as:

$$\hat{\rho}_q = \alpha_q \rho_q \tag{3}$$

3.1. Conservation of mass

The continuity equation for phase 'q' can be written as:

$$\frac{\partial}{\partial t}\left(\alpha_q \rho_q \vec{v}_q\right) + \nabla \cdot \left(\alpha_q \rho_q \vec{v}_q\right) = \sum_{p=1}^{n} (\dot{m}_{pq} - \dot{m}_{qp}) + S_q \tag{4}$$

3.2. Conservation of momentum

The momentum balance for phase 'q' gives:

$$\frac{\partial}{\partial t}\left(\alpha_q \rho_q \vec{v}_q\right) + \nabla \cdot \left(\alpha_q \rho_q \vec{v}_q \vec{v}_q\right) \tag{5}$$
$$= -\alpha_q \nabla p + \nabla \cdot \bar{\bar{\tau}}_q + \alpha_q \rho_q \vec{g} + \sum_{p=1}^{n} (\vec{R}_{pq} + \dot{m}_{pq}\vec{v}_{pq} - \dot{m}_{qp}\vec{v}_{qp}) + (\vec{F}_q + \vec{F}_{lift,q}$$
$$+ \vec{F}_{wl,q} + \vec{F}_{vm,q} + \vec{F}_{td,q}$$

where

$$\bar{\bar{\tau}}_q = \alpha_q \mu_q \left(\nabla \vec{v}_q + \nabla \vec{v}_q^T\right) + \alpha_q \left(\lambda_q - \frac{2}{3}\mu_q\right) \nabla \cdot \vec{v}_q \bar{\bar{I}} \tag{6}$$

$$\vec{R}_{pq} = -\vec{R}_{pq};\ \vec{R}_{qq} = 0 \tag{7}$$

$$\sum_{p=1}^{n} \vec{R}_{pq} = \sum_{p=1}^{n} K_{pq}(\vec{v}_p - \vec{v}_q) \tag{8}$$

3.3. Closure models

Due to the continuum assumption and the averaging property of the Eulerian-Eulerian model, the stress tensor of the solid phase is not explicitly accounted for and the discrete character of the dispersed phase is often lost; hence, the Kinetic Theory of Granular Flow (KTGF) is used to obtain the solid phase kinematic properties. By so doing, additional closure models are required in order to re-capture important aspects of particle behaviour (Shah et al., 2015; Liu, 2014).

Interphase drag and granular viscosity are the major phenomena, which are often considered in order to obtain solutions well representative of the actual flow physics. In addition, the stress tensor of the solid phase contains shear and bulk viscosities arising from particle momentum exchange due to translation and collision (Fluent, 2017). The frictional viscosity component can also be included to accurately model conditions of very high solid volume fraction. Hence, the total viscosity of the solid phase is calculated as:

$$\mu_S = \mu_{S,col} + \mu_{S,kin} + \mu_{S,fr} \tag{9}$$

3.3.1. Collisional viscosity

The collisional component of the shear viscosity proposed by Gidaspow (1994) is modelled as:

$$\mu_S = \frac{4}{5}\alpha_S \rho_S d_S g_{0,SS}(1 + e_{SS})\left[\frac{\Theta_S}{\pi}\right]^{1/2} \alpha_S \tag{10}$$

3.3.2. Kinetic Viscosity

According to Gidaspow, (1994):

$$\mu_{S,kin} = \frac{10\rho_S d_S \sqrt{\Theta_S \pi}}{96\alpha_S(1 + e_{SS})g_{0,SS}}\left[1 + \frac{4}{5}g_{0,SS}\alpha_S(1 + e_{SS})\right]^2 \alpha_S \tag{11}$$

3.3.3. Bulk viscosity

The bulk viscosity accounts for the resistance the particles possess against compression and expansion during flow. Lun et al. (1984) described this effect as:

$$\lambda_S = \frac{4}{3}\alpha_S^2 \rho_S d_S g_{0,SS}(1 + e_{SS})\left[\frac{\Theta_S}{\pi}\right]^{1/2} \tag{12}$$

3.3.4. Frictional viscosity

The frictional component of the total solids viscosity is applicable to dense flows at low shear, in which the solids volume fraction approaches the packing limit and is calculated using the model proposed by Schaeffer (1987).

$$\mu_{S,fr} = \frac{p_S \sin\phi}{2\sqrt{I_{2D}}} \tag{13}$$

3.3.5. Particle drag model

The model proposed by Gidaspow (1994) combines the Wen and Yu (1966) model and the Ergun equation for accurate solutions. The Gidaspow interphase drag model can also be used for large volume fractions, especially at high ROPs. This flexibility is not offered by the Wen and Yu drag model.

When $\alpha_l > 0.8$, the fluid-solid exchange coefficient, K_{sl}, is calculated as:

$$K_{sl} = \frac{3}{4} C_D \frac{\alpha_S \alpha_l \rho_l |\vec{v}_s - \vec{v}_l|}{d_s} \alpha_l - 2.65 \tag{14}$$

where

$$C_D = \frac{24}{\alpha_l Re_s}[1 + 0.15(\alpha_l Re_s)^{0.687}] \tag{15}$$

When $\alpha_l \leq 0.8$,

$$K_{sl} = \frac{150\alpha_S(1-\alpha_l)\mu_f}{\alpha_l d_s^2} + 1.75\frac{\alpha_s \rho_l |\vec{v}_s - \vec{v}_l|}{d_s} \tag{16}$$

3.3.6. Particle lift model

The Saffman-Mei lift force model was adopted in ANSYS-FLUENT (Saffman, 1968; Mei and Klausner, 1994). Its applicability to spherical and slightly distorted particles make it more robust compared to the Moraga (1999) lift force model.

$$C_l = \frac{3}{2\pi\sqrt{Re_\omega}} C'_l \tag{17}$$

$$C'_l = 6.46 \; and \; 0 \leq Re_p \leq Re_\omega \leq 1 \tag{18}$$

Mei and Klausner (1994) extended the model to a higher range of particle Reynold numbers (Re_p). Hence, the Saffman-Mei model can be empirically represented as:

$$C_l = \frac{3}{2\pi\sqrt{Re_\omega}} C'_l \tag{19}$$

$$C'_l = \begin{cases} 6.46 \times f(Re_p, Re_\omega) & Re_p \leq 40 \\ 6.46 \times 0.0524(\tilde{\beta} Re_p)^{1/2} & 40 < Re_p < 100 \end{cases} \tag{20}$$

where

$$\tilde{\beta} = 0.5(Re_\omega / Re_{p)} \tag{21}$$

$$f(Re_p, Re_\omega) = (1 - 0.3314\tilde{\beta}^{0.5})e^{-0.1Re_p} + 0.3314\tilde{\beta}^{0.5} \tag{22}$$

$$Re_p = \frac{\rho_q |\vec{V}_q - \vec{V}_p| d_p}{\mu_q} \tag{23}$$

$$Re_\omega = \frac{\rho_q |\nabla \times \vec{V}_p| d_p^2}{\mu_q} \tag{24}$$

The finite volume technique was implemented for the discretisation of the flow equations in the ANSYS-FLUENT solver (version 17.1). The capability of this discretization scheme in ensuring the conservation of mass and momentum at the elementary control volume and global level (over entire flow geometry), makes it physically consistent and hence more suitable compared to other discretization schemes. Pressure-Velocity coupling was effected using the Phase Coupled SIMPLE

scheme and the momentum equations were discretised using the QUICK routine due to its good performance on hexahedral grids (Pereira et al., 2007). Numerical solutions of the discretised equations and accompanying initial and boundary conditions were obtained after several iterations. The parallel computing feature of the software was activated for faster convergence on four processing cores. A computer with the following specifications was used to run all simulations in this work: (Windows 7, 64-bit operating system, with 16GB RAM, and Quad-Core-i7 processor at 3.40GHz). The tolerance factor was set to 10^{-3} for the continuity and 10^{-4} for all other equations. Fig. 3 explains the numerical simulation procedure required to replicate experimental data and obtain fully converged results.

3.4. Fluid rheology

The drilling fluid adopted is a mixture comprising of 350 ml Water, 22.5 g of Bentonite and 2.5 g of Xanthan gum. Experimental flow properties of the non-Newtonian drilling fluid were obtained from the work of Al-Kayiem et al. (2010). The power law model was used to describe the fluid rheology using the least squares curve fitting method as shown in Eq. 25. Water is also tested comparatively with the drilling mud for a few case studies in order to demonstrate the effectiveness of a non-Newtonian fluid in particle transport during drilling operations.

$$\tau = K\gamma^n \tag{25}$$

Table 1 summarizes the fluid and particles properties used as simulation input parameters; some of which are based on experimental studies of Chen et al. (2007) and Duan et al. (2010).

Table 1. Simulation input parameters

	Drilling Mud	**Water**
Geometry		
Drill pipe diameter (m)	0.0889	0.0889
Hole diameter (m)	0.1463	0.1463
Computational Length (m)	14	14
Particle properties (spherical)		
Cuttings diameter (m)	0.003	0.003
Cuttings density (kg.m^{-3})	2610	2610
Fluid properties		
Density (kg.m^{-3})	1036.5	998.5
Consistency index, K (Pa.s^n)	22.52	0.00103
Flow behaviour index (n)	0.151	1
Drilling variables		
ROP (ft.hr^{-1})	50, 75, 100	50
Fluid circulation velocity (ft.s^{-1})	2, 3, 4, 5	4
Flow regime	Steady state laminar	Steady state laminar
Drill pipe rotation (rpm)	0, 70, 140	0, 70, 140
Hole eccentricities (e)	0, 0.4, 0.8	0, 0.4, 0.8
Hole inclination from vertical (degrees)	0, 20, 40, 60, 90	90

3.5. Annular flow geometry

The flow system considered in this study consists of an inner rotating drill pipe with a diameter of 3.5 in (0.0889 m), and a stationary outer pipe representing the wellbore with diameter 5.76 in (0.1463 m). A pipe length of 14 m was selected after calculating the maximum entrance length - L_e (the length required for fully developed flow for all fluid circulation velocities). Shook and Roco (1991) proposed a correlation for calculating the entrance length in the case of single-phase laminar flow as:

$$\frac{L_e}{D} = 0.062 Re_t \tag{26}$$

where

$$Re_t = \frac{\rho_f \tilde{u}_m D}{\mu_f} \tag{27}$$

No correlation for predicting L_e exists for solid-liquid flow, however, Eq. (26) can be used as an approximation of the required entrance length, where D becomes the difference between the drill pipe diameter and the hole diameter. Three separate flow configurations are studied with eccentricities of 0, 0.4 and 0.8 respectively (concentric, moderately eccentric and highly eccentric annuli – Fig. 2).

$$e = \frac{2\delta}{D_{hole} - D_{drillpipe}} \tag{28}$$

3.6. Computational mesh and grid independence study

Structured hexahedral meshes were adopted in all flow configurations comprising of approximately 0.93 - 4.5 × 10^6 elements. Edge sizing and face meshing methods were implemented at the inlet and outlet boundaries, thus providing a good resolution capable of capturing boundary conditions. It was essential to ensure high orthogonality and low skewness in the mesh; thus, the number of external pipe divisions were same as those of the internal pipe. Table 2 shows the mesh quality parameters for the different flow configurations studied.

In order to determine the optimum number of elements for which an accurate solution can be obtained at the expense of least computational resources, a mesh/grid independence study was necessary for all pipe eccentricities considered (Fig. 4). Flow simulation was carried out in a horizontal annulus without pipe rotation at a fluid velocity of 1.22 $m.s^{-1}$. The study was carried out at different total face divisions while keeping the number of axial divisions constant. The total number of face divisions is calculated by multiplying the number of edge divisions by radial face divisions. Fig. 2a-c show that the concentric flow configuration requires more elements compared to the eccentric annuli for a solution independent of the grid size.

Table 2. Computational mesh properties

	Concentric Hole e = 0	**Eccentric Hole - 1 e = 0.4**	**Eccentric Hole - 2 e = 0.8**
Edge divisions	50	50	50
Radial face divisions	30	20	20
Total face divisions	1500	1000	1000
Number of elements	2,842,500	1,952,280	2,109,400
Number of nodes	11,658,850	8,105,124	8,757,296
Minimum skewness	0.0391	0.0333	0.0352
Maximum skewness	0.0451	0.1443	0.2091
Average skewness	0.0407	0.0896	0.1001
Minimum orthogonality	0.9981	0.9751	0.9041
Maximum orthogonality	0.9987	0.9988	0.9987
Average orthogonality	0.9985	0.9897	0.9713

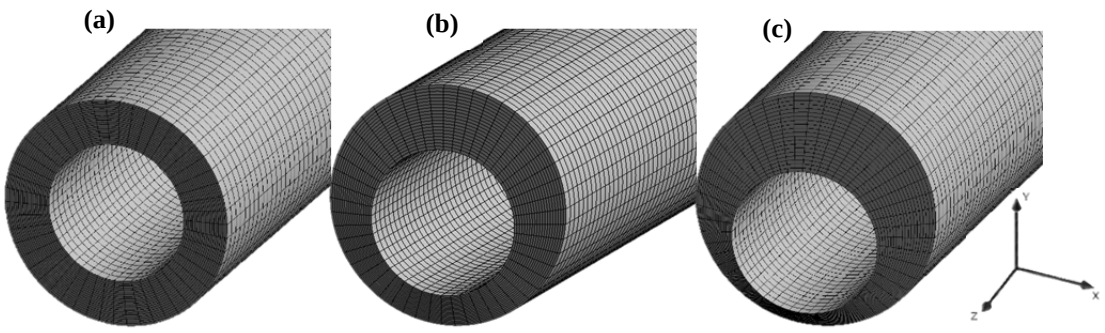

Fig. 2. Computational Mesh for the different flow configurations (a) concentric (b) moderately eccentric (c) highly eccentric; these capture the attainable drillpipe positions relative to the borehole walls.

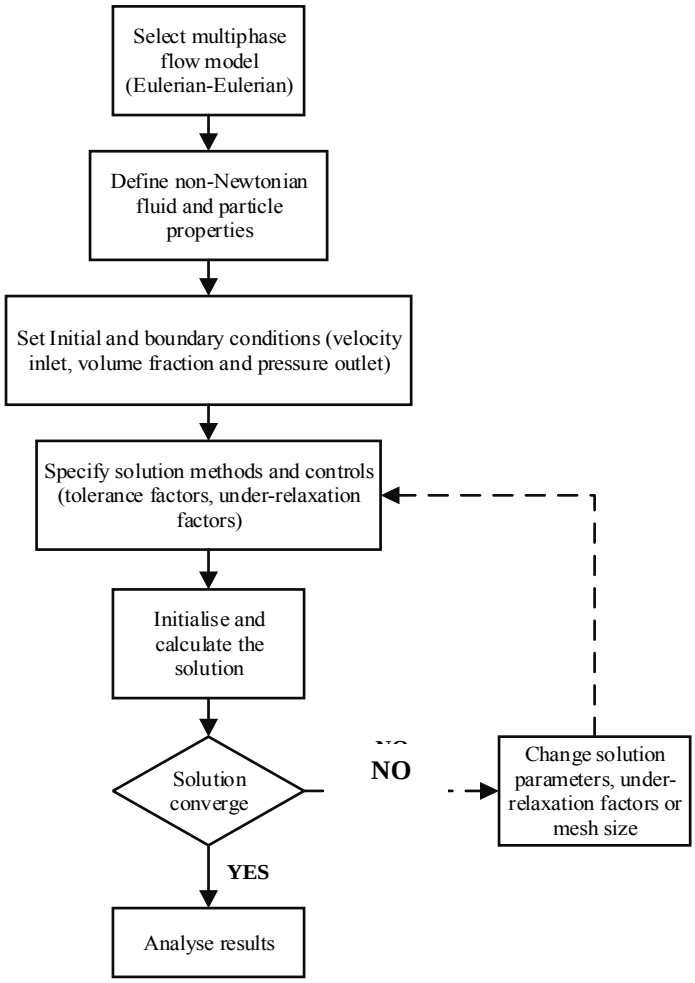

Fig. 3. General simulation procedure using the Eulerian-Eulerian multiphase flow model.

Besides the flow physics, the under-relaxation factors are major determinants of the speed of convergence and stability of steady state CFD simulations. These were carefully tuned until most appropriate values were obtained. In all cases except when water was used as the drilling fluid, each simulation converged within 30 mins. The difficulties observed with water resulted in double the run time required for the non-Newtonian drilling fluid cases.

3.7. CFD model validation

In order to validate the CFD model, several experimental observations were compared with the cuttings concentrations, cuttings velocity and pressure losses predicted. Table 3 summarizes the simulation input parameters for all three experimental studies. The inlet cuttings concentration was determined using the methods of Larsen et al. (1997) and Ozbayoglu et al. (2010) for experiments in which cuttings bed porosity was measured (Eq. 29) and when it was ignored (Eq. 30).

$$C = \frac{ROP\ (1-\varphi)}{\left[1-\frac{D_{pipe}}{D_{hole}}\right]^2 V_{cut}} \tag{29}$$

$$C = \frac{ROP}{\left[1-\frac{A_{pipe}}{A_{hole}}\right] V_{cut}}\text{; also calculated as: } C = \frac{ROP(A_{bit})}{CTR \times Q} \tag{30}$$

where

$$\mathrm{C} = \frac{\text{Net volume occupied by particles}}{\text{Total volume of annulus}} \times 100 \tag{31}$$

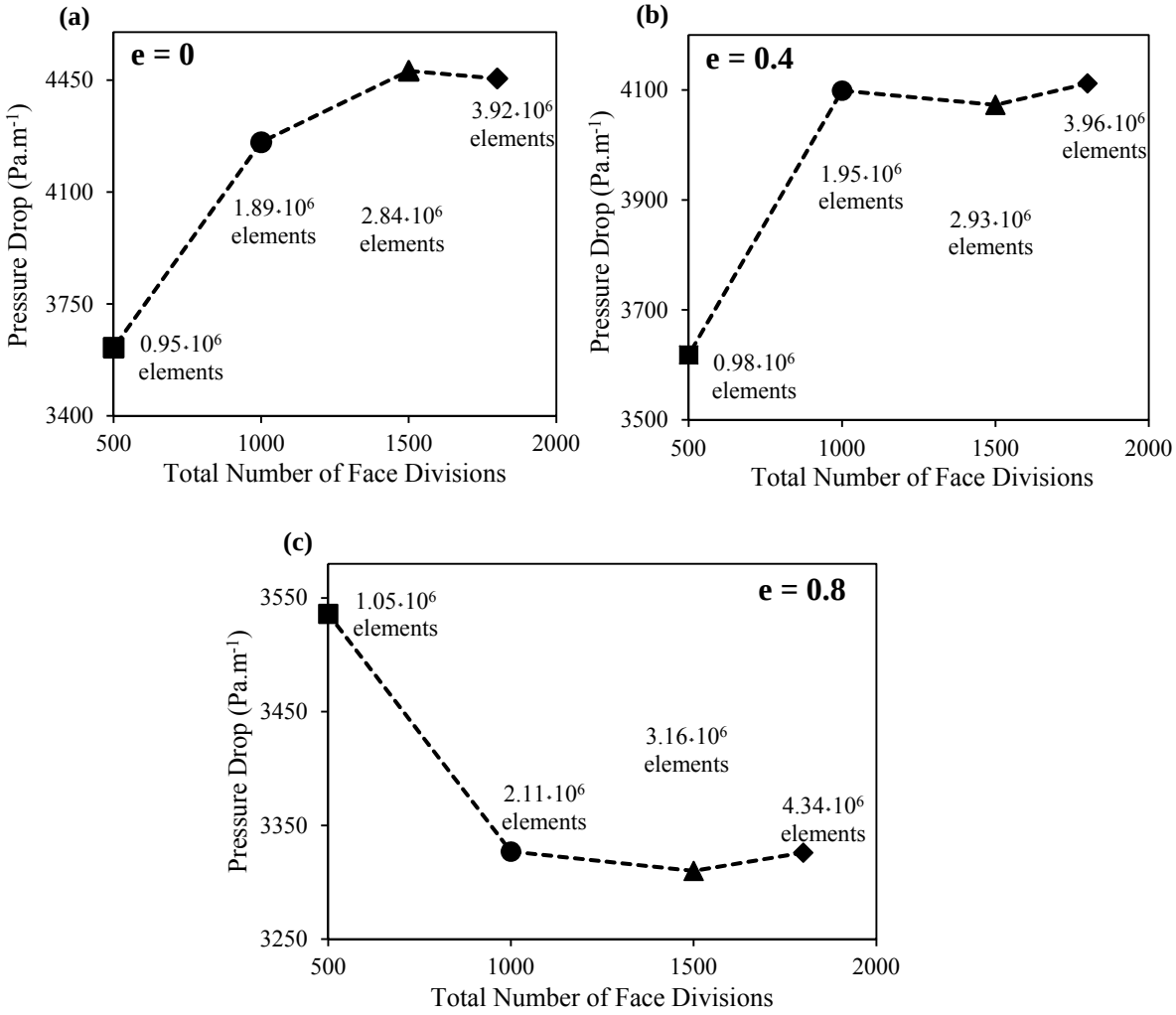

Fig. 4. Grid Independence Study (a) e = 0, (b) e = 0.4, (c) e = 0.8 at 0 rpm, 1.22 $m.s^{-1}$ fluid velocity in a horizontal annulus.

Fig. 5a-d show results of CFD predictions for the pressure losses, cuttings concentration and cuttings velocity in the annulus with average percentage errors between 2% and 11% for all cases considered. The predictive ability of the CFD model used in the present study is thus confirmed by its congruence with experimental data. Cuttings lag velocity was the most difficult parameter to predict using the Eulerian model (Fig. 5e & 6c). Yilmaz (2012) also predicted the experimental results of cuttings bed velocity (Garcia-Hernandez et al., 2007) using the DPM one-way coupling of the particle-fluid interactions. The mean absolute error obtained was 8.5%. A lower error of 4.2% was obtained in the work of Demiralp (2014) in which interparticle collisions were accounted for, using the DEM technique. The present work however, produced a mean error of 10.8% using the Eulerian model. The relatively higher error observed in this work can be attributed to the inherent approximation of the discrete phase as a continuum phase in the Eulerian-Eulerian model. Thus, interparticle collision using the Discrete Element Method (DEM) could be adopted with the Discrete Phase Model for better predictions; however, this is bound to prohibitively increase the computational run time considering the relatively large flow domain implemented in this work.

Table 3. Experimental data summary used for model validation

	Osgouei (2010)	**Han et al. (2010)**	**Chen et al. (2010)**	**Garcia Hernandez et al. (2007)**	**Duan et al. (2006)**	**Sorgun (2010)**
Flow Geometry						
Drill pipe diameter (m)	0.0470	0.030	0.0889	0.1143	0.1143	0.0457
Hole diameter (m)	0.0739	0.044	0.1463	0.2032	0.2032	0.0739
Computational Length (m)	6.40	1.80	22.25	30.48	30.48	3.66
Particle Properties						
Cuttings density ($kg.m^{-3}$)	2761.4	2550	2610	2610	2610	2610
Cuttings diameter (m)	0.00201	0.001	0.003	0.004	0.0014	0.003
Cuttings bed porosity (%)	-	-	38	-	-	-
Fluid Properties						
Fluid type	Water	0.4% CMC sol	80% quality foam	Water	Water	Water
Density ($kg.m^{-3}$)	998.5	998.5	285	998.5	998.5	998.5
Consistency index, K ($Pa.s^n$)	0.001	0.048	3.385 (Rooki et al., 2015)	0.001	0.001	0.001
Flow behaviour index (n)	1.0	0.75	0.439 (Rooki et al., 2015)	1.0	1.0	1.0
Drilling variables						
ROP ($ft.hr^{-1}$)	80	62	50	30	30	30
Fluid circulation velocity ($m.s^{-1}$)	1.524 – 2.743	0.32 – 0.66	0.3 – 1.83	1.1 – 1.5	1.1 – 1.5	0.64 – 1.20
Flow regime	Steady state turbulent	Steady state laminar	Steady state laminar & turbulent	Steady state laminar	Steady state laminar	Steady state laminar
Drill pipe rotation (rpm)	0	0	0	0	0	0, 120
Hole eccentricities (e)	0.623	0	0	0.8	0.8	1
Hole inclination from vertical (^{o})	90	0 - 60	90	90	90	90
Cuttings injection rate ($kg.s^{-1}$)	0.0803	0.0204	0.115	0.358	0.215	0.0284
Temperature (K)	298	298	299.8	-	298	-
Operating Pressure (psig)	0	0	100	-	0	-

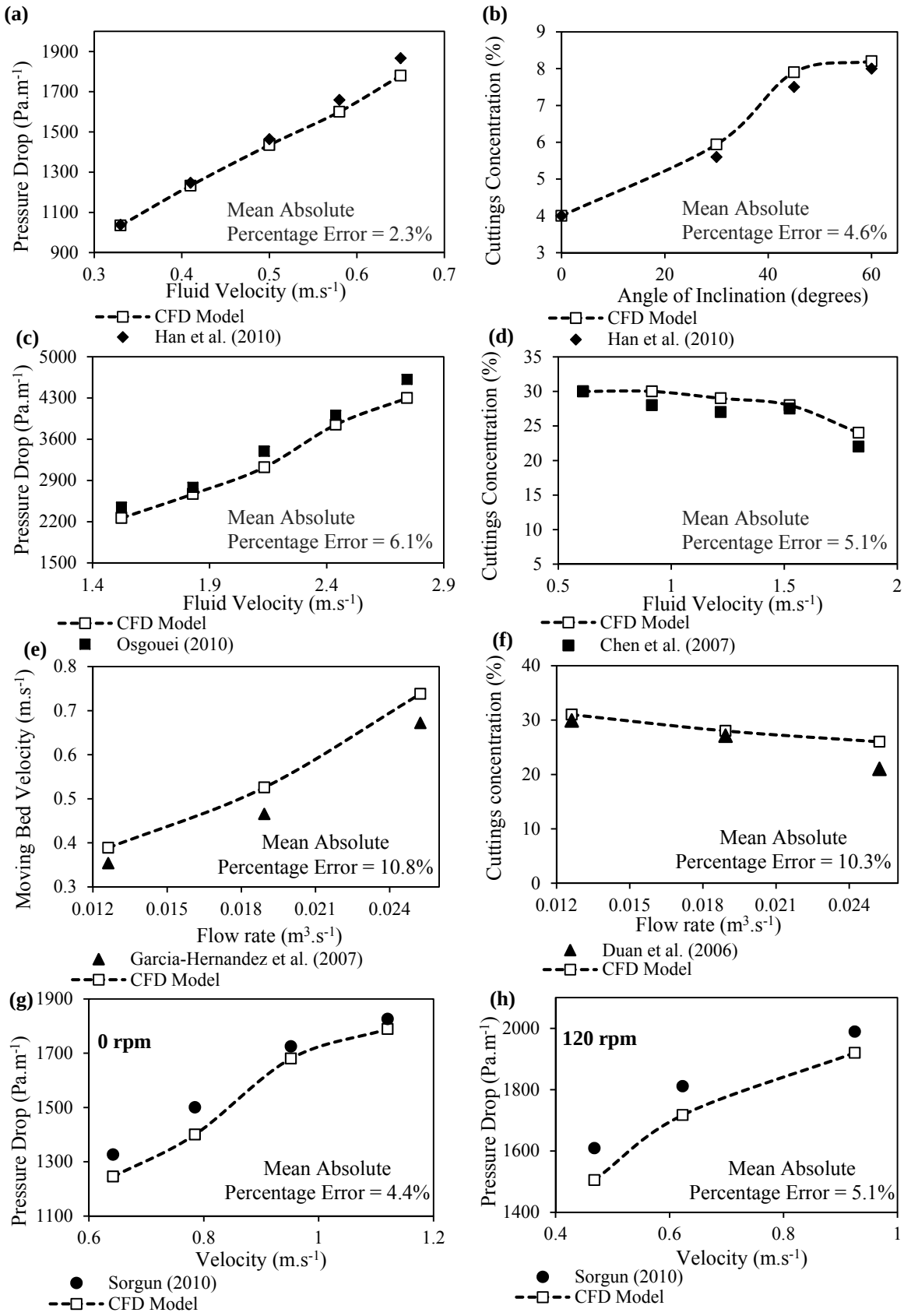

Fig. 5. Validation of CFD model against experimental data.

Table 4. Comparison between experimental data and model predictions of cuttings concentration and cuttings velocity

Han et al. (2010)			Chen et al. (2007)			Duan et al. (2006)			Garcia-Hernandez (2007)		
Cuttings concentration			Cuttings concentration			Cuttings concentration			Cuttings velocity		
Exptl. (%)	CFD (%)	RE (%)	Exptl. (%)	CFD (%)	RE (%)	Exptl. (%)	CFD (%)	RE (%)	Exptl. ($m.s^{-1}$)	CFD ($m.s^{-1}$)	RE (%)
4.00	4.01	0.25	30.0	30.02	0.33	29.90	31.00	3.68	0.35	0.39	9.86
5.60	5.94	6.07	28.0	29.85	6.61	27.10	28.00	3.32	0.47	0.53	12.87
7.50	7.90	5.33	27.0	29.10	7.78	21.10	26.00	23.81	0.67	0.74	9.79
8.00	8.20	2.50	27.5	28.00	1.82	-	-	-	-	-	-
-	-	-	22.0	24.00	9.09	-	-	-	-	-	-

Table 5. Comparison between experimental data and model predictions of pressure drop

Han et al. (2010) 0 rpm			Osgouei (2010) 0 rpm			Sorgun (2010) 0 rpm			Sorgun (2010) 120 rpm		
Pressure drop			Pressure drop			Pressure drop			Pressure drop		
Exptl. ($Pa.m^{-1}$)	CFD ($Pa.m^{-1}$)	RE (%)	Exptl. ($Pa.m^{-1}$)	CFD ($Pa.m^{-1}$)	RE (%)	Exptl. ($Pa.m^{-1}$)	CFD ($Pa.m^{-1}$)	RE (%)	Exptl. ($Pa.m^{-1}$)	CFD ($Pa.m^{-1}$)	RE (%)
1038.0	1035.0	0.29	2443.0	2262.0	7.41	1326.0	1245.3	6.11	1609.3	1505.2	6.46
1247.1	1233.0	1.12	2782.3	2669.2	4.07	1500.4	1400.1	6.67	1811.0	1717.1	5.19
1464.2	1435.0	1.98	3393.1	3121.6	8.00	1725.0	1680.0	2.61	1989.1	1920.0	3.47
1659.1	1600.0	3.56	4003.8	3845.5	3.95	1826.1	1789.6	2.03	-	-	-
1867.0	1780.2	4.66	4614.5	4614.5	6.86	-	-	-	-	-	-

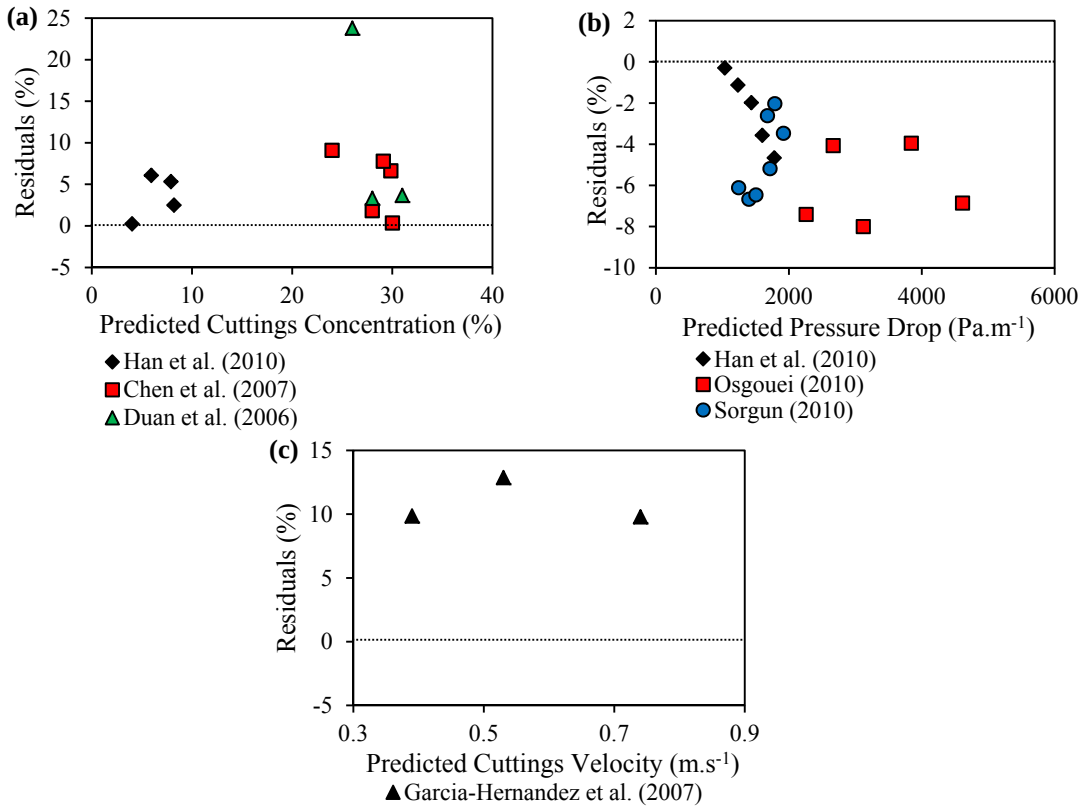

Fig. 6. Residual plots of cuttings concentration, pressure drop and cuttings velocity predictions

The relative errors (RE) between experimental results and CFD predictions are compared and summarized in Tables 4 and 5. Additionally, the residual plots (Fig. 6) illustrate that the cuttings concentration were in most cases slightly overpredicted by the Eulerian-Eulerian model. Conversely, the pressure drop predictions were in all cases, lower than the experimental results. Accurate prediction of final cuttings concentration is significantly dependent on the accuracy of the inlet cuttings volume fraction supplied to the simulator. This parameter (inlet volume fraction) is not often stated in most experimental studies and hence, must be estimated. The uncertainty in the estimation of this variable in relation to the actual experimental inlet conditions is a possible reason for the observed errors in cuttings concentration. Asides inter-particle collision, the frequency of particle collisions with the walls of the drill pipe and casing pipe, which possess some degree of roughness, affects the pressure drop predictions by the CFD model. Accounting for these effects would warrant a more complex four-way coupling of the fluid and solid momentum equations. While predictive ability is not always guaranteed by model complexity, maintaining a computationally acceptable trade-off between accuracy, run time and model simplicity is essential and thus constituted a guiding principle in this study.

Similar pressure drop predictions have been performed by Ofei et al. (2014) using the experiments of Han et al. (2010) and Osgouei (2010). The Eulerian-Eulerian model implemented in their work yielded a mean error of less than 5%. This is not far that obtained in the present study (Fig. 5a & c). Furthermore, the predictions of cuttings concentration using experimental data of Chen et al. (2007) are slightly better (Fig. 5d) than those of Reza et al. (2015) in which the mean error was somewhat less than 8%. Although the Eulerian-Eulerian model was also implemented in their work, the very fine meshes adopted for computation in this work is the obvious reason for the observed model performance.

The broad range in the fluid and solid properties, geometric and drilling parameters as shown in Table 3 is well accounted for by the simulation strategy adopted, hence further demonstrating the robustness of the CFD model. The impact of several drilling operational parameters on the cuttings removal efficiency was studied as a function of the resultant pressure drop and cuttings concentration. Contour plots of phase velocities and volume fractions are also presented in the results section.

4. Results and Discussion

4.1. Effect of fluid circulation velocity

Two important characteristics of annular solid-liquid flow are the pressure drop versus mixture velocity relationship and the resultant cuttings concentration that ensue as a result of the fluid velocity used for hole cleaning. In this study, fluid circulation velocity is varied under laminar conditions at different drill pipe rotations, eccentricities and inclination angles from the vertical. Fig. 7a-b represent the impact of fluid velocity on the pressure drop and cuttings concentration at different pipe rotations in a horizontal eccentric annulus. An increase in pressure drop is observed as the velocity increases for all pipe rotations; however, this increase is more pronounced when the drill pipe is stationary. For example, pressure drop increased from 1886 $Pa.m^{-1}$ at 0.61 $m.s^{-1}$ to 2223 $Pa.m^{-1}$ at 1.524 $m.s^{-1}$ without drill pipe rotation. This is a more significant increase compared to the slight increase from 2163 $Pa.m^{-1}$ to 2239 $Pa.m^{-1}$ observed at 70 rpm within the same velocity range. Drill pipe rotation aids cuttings removal according to Fig. 7b, but this occurs at the expense of a higher pressure drop. Furthermore, the narrowly spaced cuttings concentration trends are indicative of the fact that increasing drill pipe rotation has minimal impact on cuttings concentration.

Despite the application of several technologies that seek to ensure a centralised drill pipe during drilling operations, the impact of gravity and mechanical vibrations often cause the hole configurations to vary significantly from concentric to fully eccentric. Fig. 7c-d represent the impact of varying eccentricities on the pressure drop and cuttings concentration. An eccentric hole configuration yields a lower pressure drop compared to a concentric hole, and the magnitude of this reduction increases with a higher eccentricity of 0.8. This reduction in pressure drop can be attributed to the decreased mixture velocity encountered at the narrower part of the annulus. Furthermore, a

more eccentric hole implies a bigger suspended layer area and thus a lower resistance to flow. Unlike the Cuttings Transport Ratio (CTR), cuttings concentration is a better indication of the cuttings transport efficiency especially in deviated wellbores when cuttings buildup or bed formation occurs (Iyoho et al., 1986). It is shown in Fig. 7d that cuttings concentration is lower when the inner drill pipe is concentric with the outer pipe (wellbore) and buildup of cuttings increases as the configuration becomes more eccentric. At a circulation velocity of 0.61 $m.s^{-1}$ the cuttings concentration increases by 51% when the hole configuration changes from 0 to 0.8 eccentricity. Thus, the best carrying capacity of the fluid occurs with reducing eccentricity. The disparity between the cuttings concentration observed for both 0.4 and 0.8 hole eccentricities decreases as the fluid circulation velocity increases. This further explains the dominating impact of increasing fluid velocity on transport efficiency compared to other drilling variables.

Cuttings deposition could also occur at the bottom of the drill pipe in the axial direction when fluid velocity is not sufficient to overcome the axial or radial components of the gravitational force acting in the flow domain due to hole inclination. An important observation shown in Fig. 7e is the slightly decreasing pressure drop with increasing fluid velocity at near vertical annular configurations (0^o and 20^o). Conversely, pressure drop slightly increases with fluid velocity as the inclination from the vertical increases (40^o and 60^o). The relative contributions of gravity and friction to the overall pressure drop at different inclination angles is a possible explanation for the observed pressure drop trends. As seen in Fig. 7f, cuttings concentration increased from 10% to 14% as the hole configuration changed from an inclination of 0^o to 40^o at 1.22 $m.s^{-1}$. This change in concentration was accompanied by a 15% decrease in pressure drop. The higher pressure drop values obtained at near vertical configurations represent the enormous power requirements required for good hole cleaning. The implementation of deviated and horizontal well drilling thus implies that a lower fluid pumping requirement is needed but with an increased in-situ cuttings concentration. The results of Fig. 7e-f thus explain the fact that a higher circulation fluid velocity is required in deviated wellbores in order to maintain continuous removal of drill cuttings.

4.2. Effect of drill pipe rotation

Fig. 8a-7d show the impact of drill pipe rotation on pressure drop and cuttings concentration at different penetration rates and hole eccentricities (e). A slightly increasing trend in pressure drop is observed with increase in rotation for both cases when ROP and eccentricity were varied. This behavior can be explained by the centrifugal forces, shear instabilities and unstable flow that ensue as a result of a rotating drill pipe (Demiralp, 2014). Also, increasing friction, velocity fluctuation and collision between particles and walls and particles themselves are major factors that contribute to the pressure drop increase. Flow through the concentric annular configuration experienced a higher pressure drop compared to the other eccentric flow geometries. The predominance of shear thinning effects over inertial effects during rotation, and the inevitable viscosity reduction especially in the narrow parts of the eccentric annulus (Demiralp, 2014), is a plausible explanation for the reduced pressure drop. A remarkably high pressure drop was observed (Fig. 8a) when the penetration rate was $100ft.hr^{-1}$. This is due to the increased mixture density and bulk viscosity following the corresponding increase in cuttings concentration (Fig. 8b). The change in cuttings concentration with pipe rotation was more sensitive to ROP than to eccentricity. At a constant ROP of $100ft.hr^{-1}$, the cuttings concentration decreased from 30% to 13.7% as drill pipe rotation increased from 0 rpm to 140 rpm; whereas, the decrease in cuttings concentration due to increased rotation (0 rpm to 140 rpm) was only from 14.8% to 13.9 % at an eccentricity of 0.8 (Fig. 8d). As explained in section 4.1, a concentric annulus always favors cuttings removal; this effect is seen in the reduced concentration values for the concentric flow configuration in Fig. 8d. Furthermore, Fig. 8d illustrates that when no pipe rotation was included, cuttings concentration increased from 6.8% to 14.8% as the flow domain changed from moderately eccentric (e=0.4) to highly eccentric (e=0.8); this explains the cleaning difficulty that ensues as a result of increased hole eccentricity.

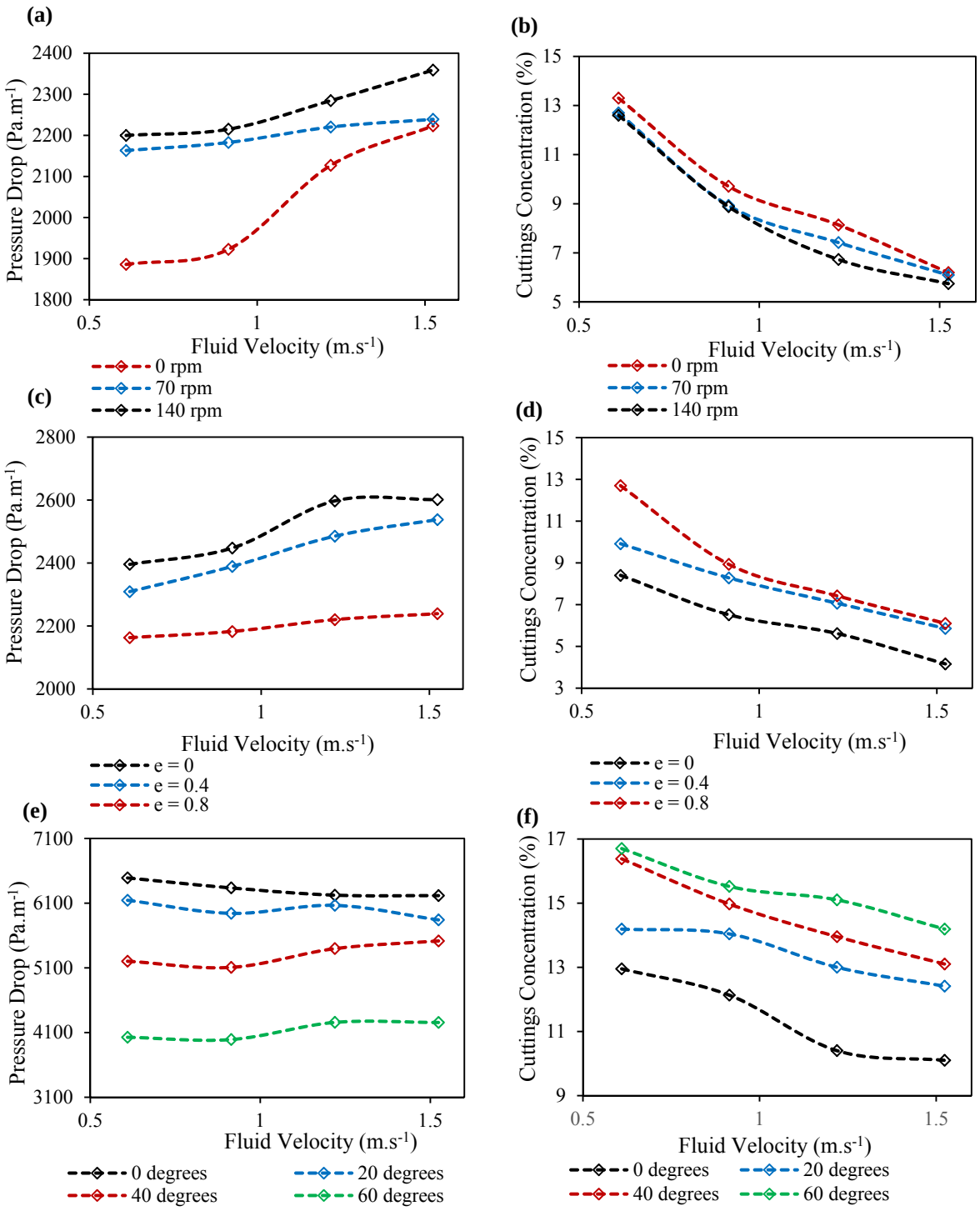

Fig. 7. Effect of fluid circulation velocity on cuttings concentration and pressure drop at: e = 0.8, 50 ft.hr^{-1}-ROP, 90^{o} – (a,b); 70 rpm, 50 ft.hr^{-1}-ROP, 90^{o} – (c,d); e = 0.8, 70 rpm, 50 ft.hr^{-1}-ROP – (e,f).

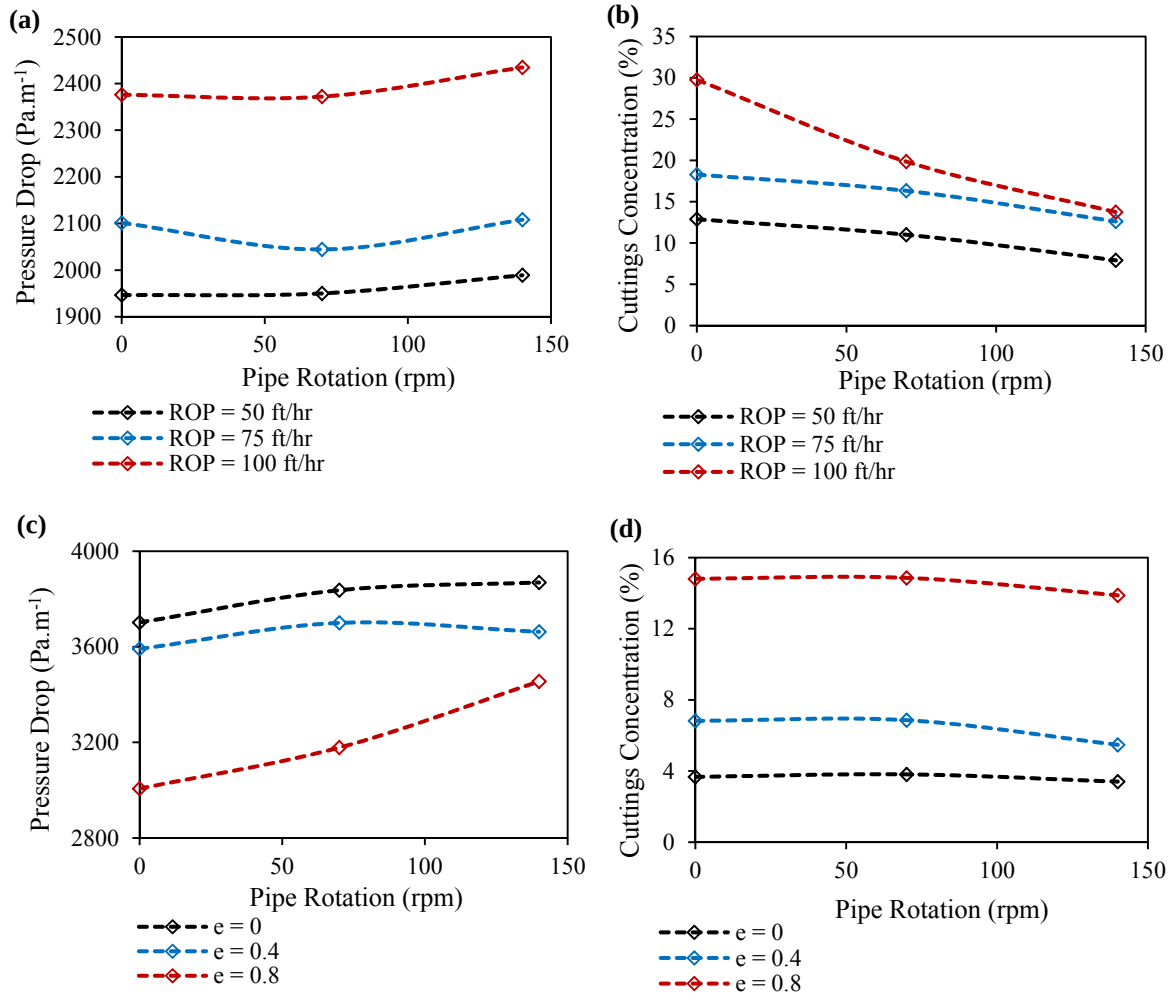

Fig. 8. Effect of drill pipe rotation on concentration and pressure drop at: V_{mud} = 1.22 m.s^{-1}, e = 0.8, 90^{o} – (a, b); V_{mud} = 1.22 m.s^{-1}, 50 ft.hr^{-1} ROP, 90^{o} – (c, d).

4.3. Effect of Rate of Penetration

Fig. 9a-d illustrate the effect of increasing ROP on the pressure drop and cuttings concentration at different hole eccentricities and inclinations. It is shown that the calculated pressure drop values are generally higher in deviated and vertical wellbores (Fig, 9c) than in the horizontal cases (Fig. 9a). It is also observed in Fig. 9c that the difference in pressure drop at all rates of penetration gradually reduces as the flow orientation becomes vertical. Furthermore, the pressure drop increases from 4257 Pa.m^{-1} to 6223 Pa.m^{-1} when the flow domain changes orientation from 60^{o} inclination to a vertical condition (0^{o}) (Fig. 9c). This is inevitably due to the increased contribution of gravity which the mixture has to overcome in order to retain upward flow. According to Fig. 9b, the concentric flow domain is seen to still favor cuttings removal at the expense of a higher pressure drop compared to the eccentric cases. Similar pressure drop and cuttings concentration are observed for the highly and moderately eccentric flow conditions at 50ft.hr^{-1} (Fig. 9a-b). However, at increased penetration rates, a greater disparity is observed between the two eccentric configurations. This explains the fact that, at high penetration rates, drastic reductions in hole cleaning efficiency can be attributed to changing annular eccentricities along the entire wellbore. As shown in Fig. 9d, increasing inclination angle and penetration rate forces more cuttings towards the lower part of the annulus, thus reducing the particle lift force generated by the fluid. Also in Fig. 9d, the cuttings concentration is seen to increase from 10% to 14.6% as the ROP increased from 50ft.hr^{-1} to 100 ft.hr^{-1} at 0^{o} inclination from the vertical. With a 20^{o} change in inclination, cuttings concentration increases from 12.1% to 15.8% between 50ft.hr^{-1} and 100ft.hr^{-1} ROP respectively; this increase is consistent with all other inclination angles.

Although a high ROP is an indicator of good drill bit performance, the results show that it has to be carefully regulated to ensure that the volume of cuttings generated can be adequately and promptly cleaned by the drilling mud.

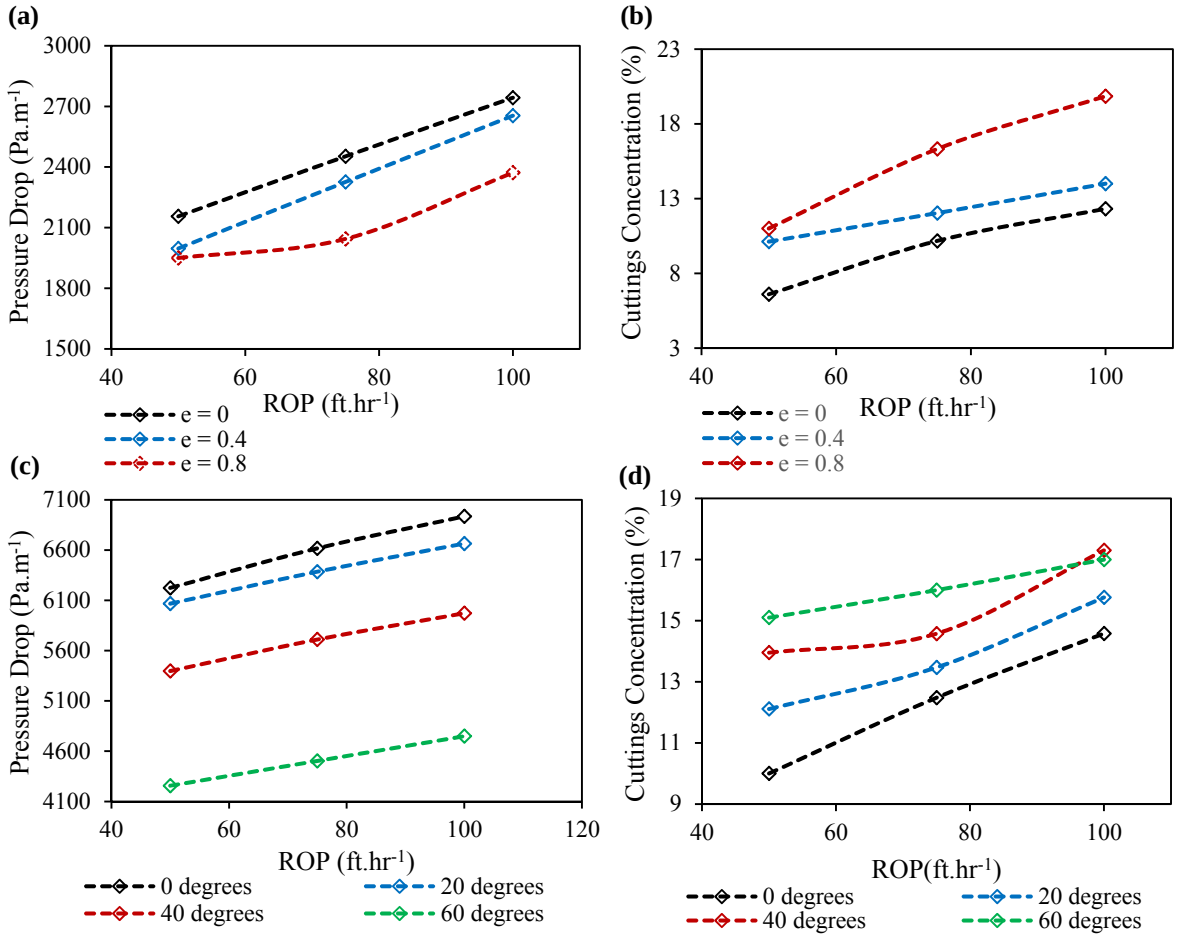

Fig. 9. Effect of Rate of Penetration on cuttings concentration and pressure drop at: V_{mud} = 1.22 m.s^{-1}, 70 rpm, 90^{o} – (a, b); V_{mud} = 1.22 m.s^{-1}, 70 rpm, e = 0.8 – (c, d).

4.4. Effect of inclination angle

Fig. 10a-d show the effect of inclination angle at different drill pipe rotations and eccentricities. In both cases of changing rotation and eccentricities, the pressure drop is seen to reduce with an increase in the inclination angle; however, the change in pressure drop is more rapid between 40^{o} and 60^{o} compared to other angles. The reverse is the case with cuttings concentration where the change in concentration between 40^{o} and 60^{o} is not as high as that observed for other angles. Experimental observations of Han et al. (2010) and Iyoho et al. (1986) also support this behavior which occurs due to the impact of gravity, thus making the transport of cuttings at these angles more difficult. Another explanation of the observed behavior (Fig. 10b and 9d) presented in the experimental observations of Iyoho et al. (1986), is the concept of particle recycling. Particles lifted from a sliding bed are not readily recycled into the high-velocity region at these inclinations angles; hence the fluid lift force can be overcome by the particles' tendency to settle. Pipe rotation had a slightly more significant impact on cuttings concentration compared to eccentricities at all inclination angles. For example, during vertical flow conditions as shown in Fig. 10b, cuttings concentration decreased from 10% to 5.9% when pipe rotation was increased from 70 rpm to 140 rpm. On the contrary, changing hole eccentricity from 0.8 to 0.4 only changed the cuttings concentration from 10% to 8.7%.

The obtained results further explain the fact that cuttings distribution and particle phase segregation in the annulus are greatly influenced by hole inclination. Asides the impact of gravity, particle inertia effects are more pronounced when the hole is inclined. Furthermore, the fairly large particles size and shape considered in this study suggests that they engage in sliding, suspended and rolling motion during transport. The dominating mechanism of particle motion depends on the hole inclination and this in turn affects the pressure drop and cuttings concentration. Since perfectly spherical particles are considered, it implies that particles will readily slide over each other as they are transported. However, this tendency is bound to reduce as the inclination from the vertical increases; thus causing an increase in the particle inertia and a corresponding gradual buildup in cuttings concentration. However, the formation of a bed of immobile cuttings is not significant due to the high carrying capacity of the fluid and the relatively low inlet volume fractions of cuttings used in the simulations. Minor particle deposits are observed when water is used as the drilling fluid in a horizontal annulus (Fig. 11a).

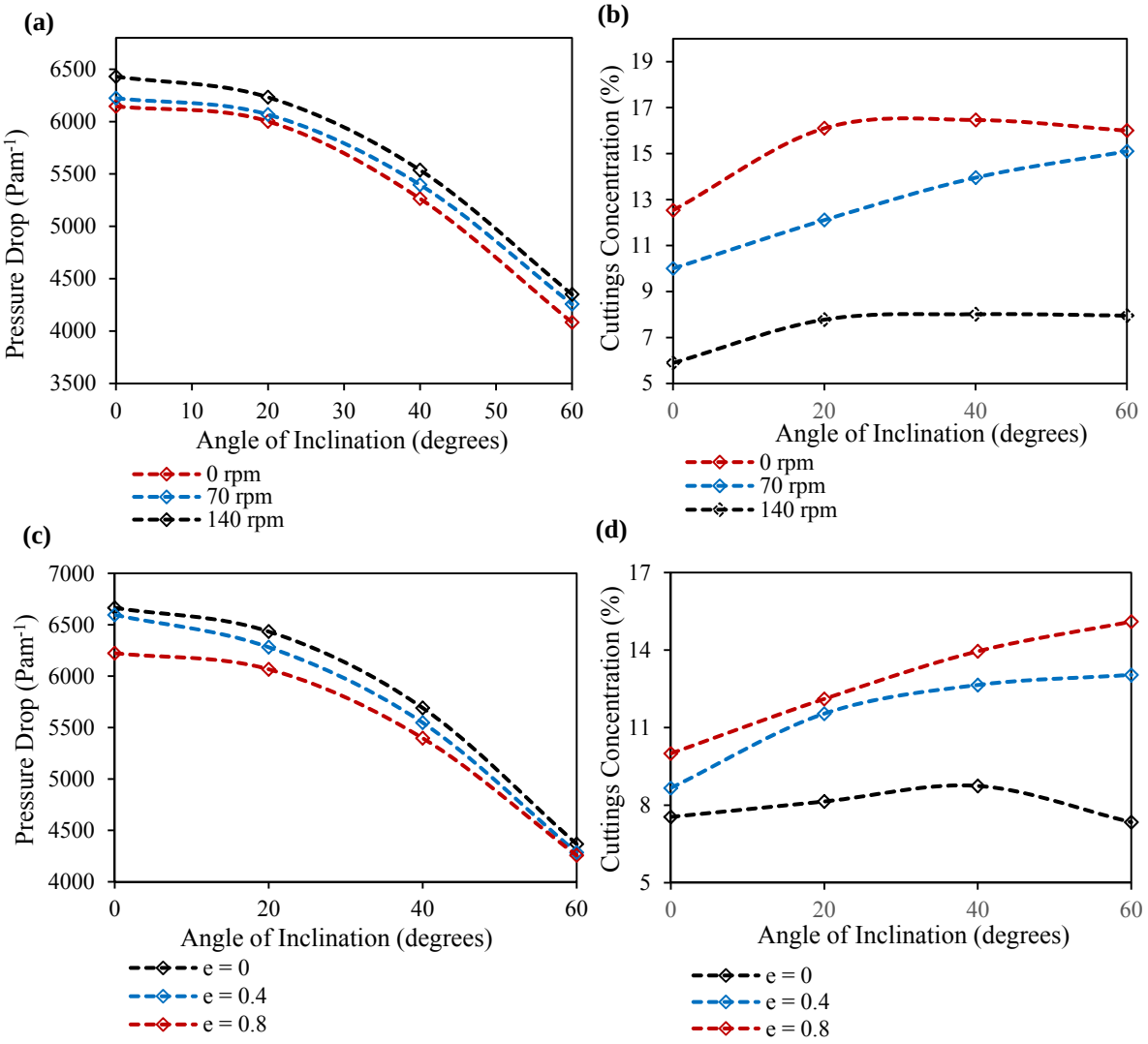

Fig. 10. Effect of inclination angle on cuttings concentration and pressure drop at: V_{mud} = 1.22 m.s^{-1}, e = 0.8, 50 ft.hr^{-1} ROP – (a, b); V_{mud} = 1.22 m.s^{-1}, 50 ft.hr^{-1} ROP, 70 rpm – (c, d).

4.5. Effect of fluid type

By comparing the carrying capacity of water (a Newtonian fluid) with the drilling mud as a function of pressure drop and cuttings concentration, it was possible to evaluate if, at any conditions, the performance of both fluids became quite similar. No such conditions were observed as shown in Fig. 11. The drilling mud clearly outperforms water which results in poor hole cleaning (depicted by the

higher cuttings concentration). While a more segregated flow pattern exists for the water transport case (Fig. 11a), a more evenly distributed transport system is noticed around the annulus when the drilling mud is used (Fig. 11b). Another important observation is the low-pressure drop values associated with the water transport case. The relatively lower water viscosity is inevitably the reason for this observation, hence its low cuttings suspension and carrying capability. It is also illustrated in Fig. 11a and b, that the transport performance of the two fluids reduces with increasing eccentricity (illustrated in the maximum cuttings concentration); thus, non-Newtonian fluid properties help overcome problems posed by inherently difficult geometries during hole cleaning.

4.6. Velocity profiles and volume fraction

The contours of cuttings volume fraction and solid velocities are shown in Fig. 12 and 13 respectively. The flowrate of drill cuttings is often higher in the paths of least resistance. However, this effect is lessened (Fig. 13) due to the excellent fluid rheological properties, high fluid circulation velocity and high cuttings injection velocity implemented. The velocity contours for the solid phase shown in Fig. 13 obey the no-slip boundary conditions implemented on the walls of the flow domain. Also, the increase in cuttings transport velocity as a result of drill pipe rotation is well illustrated in Fig. 13 at all eccentricities; hence, stagnation regions of high cuttings concentration are mitigated in the annulus. This effect of reduced concentration is not very significant, as seen in Fig. 12, in which the maximum cuttings concentration reduced from 21.8% to 20.5% in the concentric annulus, with the application of rotation.

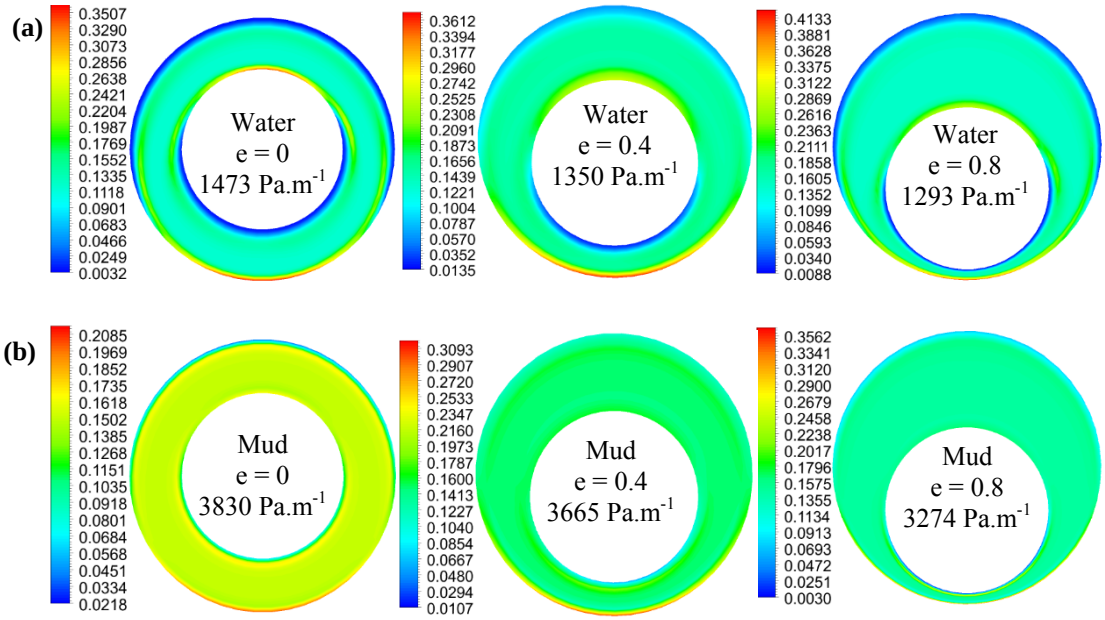

Fig. 11. Effect of fluid type on cuttings concentration at 70 rpm, V_{mud} = 1.22m.s^{-1} and 50 ft.hr^{-1} ROP in horizontal annuli.

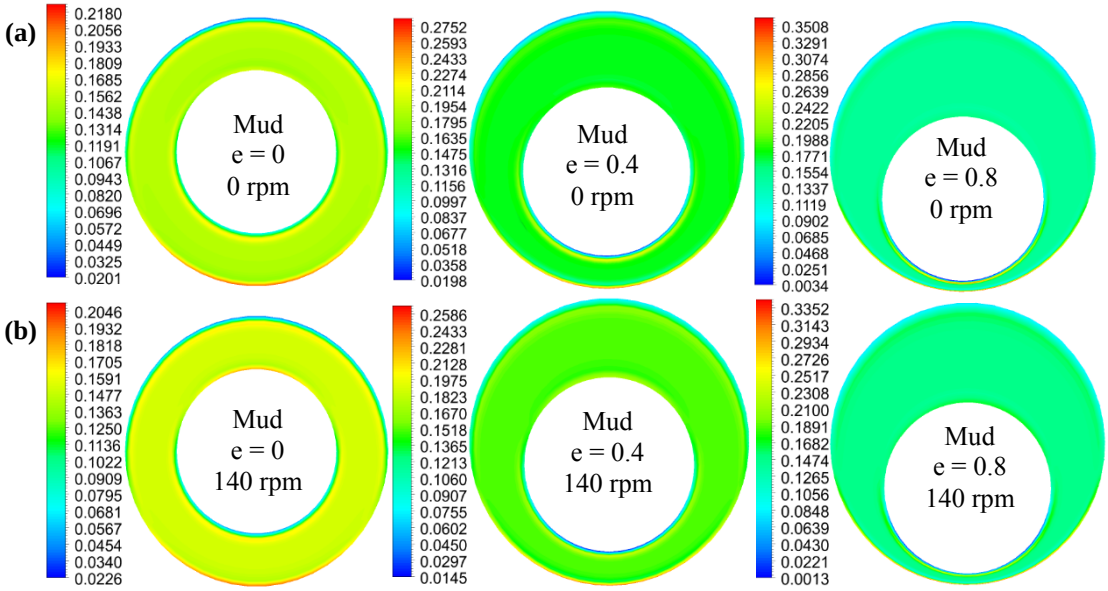

Fig. 12. Contour plots of cuttings volume fraction at different eccentricities and drill pipe rotation with drilling mud as circulation fluid (1.22 $m.s^{-1}$) in horizontal annuli.

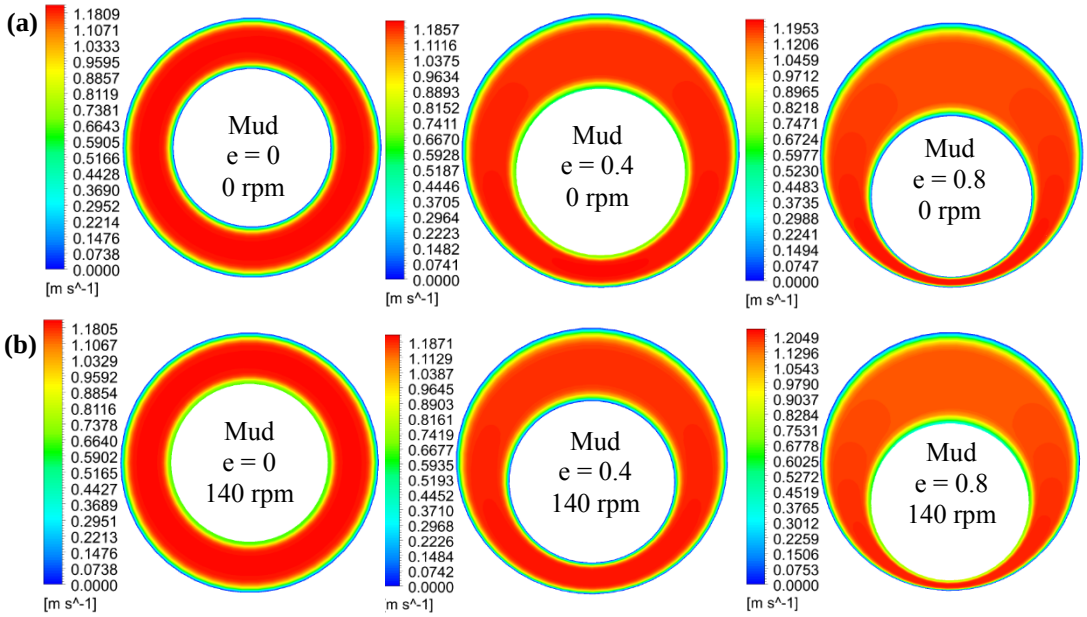

Fig. 13. Contour plots of cuttings annular velocity at different eccentricities and drill pipe rotation with drilling mud as circulation fluid (1.22 $m.s^{-1}$) in horizontal annuli.

Water, a less viscous transport fluid, inhibits an organised and stable transport of drill cuttings; this increases friction and interactions among cuttings, thus resulting in a less stable particle trajectory compared to cuttings transport using a drilling mud. There is also, a loss of kinetic energy and a slight decrease in the cuttings transport velocity, as observed Fig. 14, compared to Fig. 13 when a drilling mud is used. Essentially, the slip on the solid phase is reduced by the drilling mud due to the increased lift force it provides on the cuttings. This finding agrees with the results of Garcia-Hernandez et al. (2007) where cuttings lag in horizontal and deviated wells were determined experimentally. It can be observed in Fig. 14 that pipe rotation increases the cuttings velocity in all annular configurations

considered. The maximum cuttings velocity observed in the concentric annulus when no rotation was included was 0.9144 m.s^{-1}; an increase to 0.9468 m.s^{-1} occurs when pipe rotation was 140 rpm. This effect can be explained by the reduced drag and slip velocity, which arise as a result of the uniformity in particle trajectory with pipe rotation (Garcia-Hernandez et al., 2007).

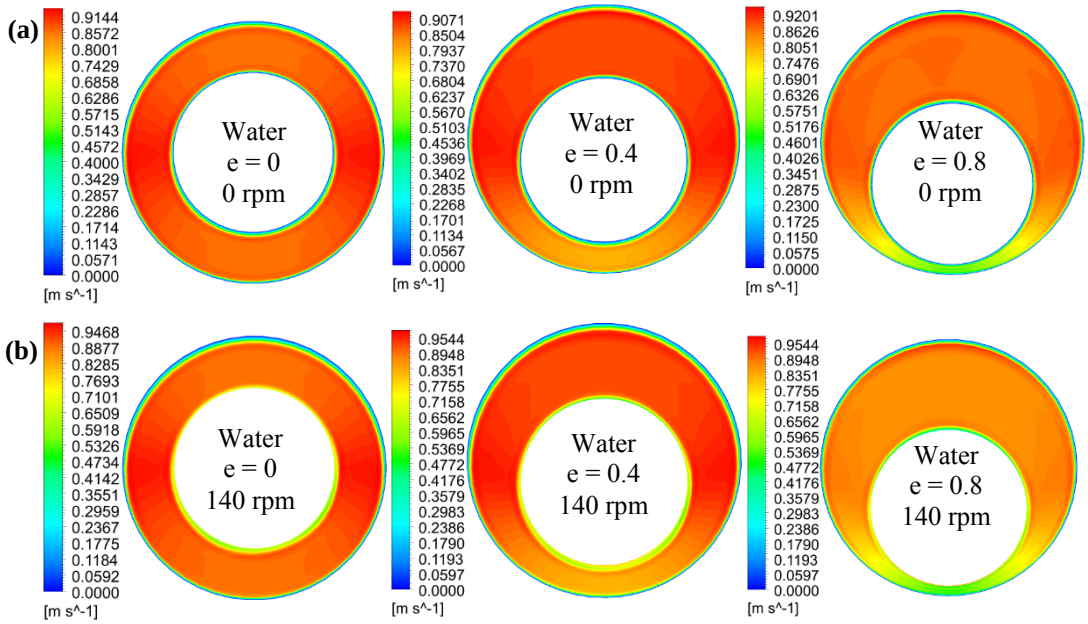

Fig. 14. Contour plots of cuttings annular velocity at different eccentricities and drill pipe rotation with water as circulation fluid (1.22 m.s^{-1}) in horizontal annuli.

5. Conclusions

This paper presents the modelling and simulation of cuttings transport phenomena during drilling operations by employing the Eulerian-Eulerian multiphase flow model. Analysis of the two-phase, solid-liquid flow was carried out under laminar, steady state and isothermal conditions in order to determine the impact of drill pipe rotation, ROP, angle of inclination, hole eccentricity and fluid circulation velocity on the pressure drop and cuttings concentration. The following conclusions can be drawn based on the observations made during this study:

- Numerical simulations of pressure drop and cuttings concentration showed good physical agreement with experimental data. Mean percentage error in pressure drop and cuttings concentration predictions were less than 11%. This illustrates the reliability of CFD simulations in replicating physical multiphase flow phenomena and consequently the validity of the model used in this work. However, uncertainties in experimental investigations and the averaging property of the RANS equations compared to DNS simulations pose flow prediction difficulties. From an operational point of view, such an error level is not likely to yield a misleading understanding of the transport phenomena. Thus, adequate planning of well trajectory, proper rheological design of drilling fluid and surface pumping requirements can be attained with the insights provided in this work.
- Fluid circulation velocity plays a crucial role in ensuring continuous cuttings removal from the annulus. Laminar flow conditions were sufficient to provide good hole cleaning with generally low cuttings concentration observed. A significant increase in annular pressure drop ensues when fluid velocity increases. Increased drag by the fluid on the particles and frictional effects are the main contributing factors to the observed phenomena.
- For most flow configurations and conditions, increasing drill pipe rotation slightly aids the cuttings removal process with accompanying slight pressure increase. For all pipe eccentricities considered, the reduction in cuttings concentration with the onset of drill pipe rotation was only 8%.

Furthermore, the additional whirling motion that occurs increases particle-particle and particle-wall collisions and is thus responsible for the pressure drop increase. Drill pipe rotation also plays a significant role in particle distributions around the annulus, which often occurs in an asymmetric pattern.

- At all conditions of transport, the cuttings concentration is lowest when the drill pipe was concentric with the outer pipe. However, pressure drop reduces with increasing eccentricity and cleaning difficulty increases as the flow domain becomes more eccentric. On the other hand, hole cleaning becomes even more difficult with increasing penetration rates due to the rapid ingress of cuttings into the annulus.
- Fluid pump pressure requirements dramatically increase as the inclination from the vertical reduces. The change in pressure drop is highest between inclination angles of 40^o and 60^o; hence, cuttings transport within these angles can be energy demanding. Similarly, cuttings concentration in the annulus could increase by 51% when the flow configuration changes from vertical to 60^o inclination. In order to limit the formation of a cuttings bed, the annular mud velocity in directional wells has to be significantly higher than in vertical wells. In cases where a well's orientation must be inclined, the velocity of the drilling fluid employed must be able to counteract the effects of gravity, which aids particle settling. It was also discovered that the effect of increasing inclination angle with increasing cuttings concentration is more significant with the onset of hole eccentricity.
- When water (a Newtonian fluid) was used for hole cleaning, particle buildup in the annulus increased compared to when the power law fluid was used. Hence, non-Newtonian fluids, (if properly designed) ensure proper hole cleaning even under flow configurations that are inherently difficult to clean.

This work was strictly limited to a steady state solid-liquid system; hence no consideration was given to the third gas phase which could occur when an aerated drilling fluid is used, or when there is gas influx from the reservoir due to the application of underbalanced drilling technology. Further work should therefore, consider steady and transient behavior of a system containing all three phases in order to better describe the cuttings transport phenomena under more complex conditions.

6. Acknowledgements:

The authors gratefully acknowledge the financial support of the University of Edinburgh via a studentship awarded to Mr E. I. Epelle. Tabulated and cited literature data suffice for reproduction of all original process simulation results and no other supporting data are required to ensure reproducibility.

7. Nomenclature and Acronyms

Latin letters

A_{pipe}	Drill pipe cross sectional area (m^2)
A_{hole}	Hole cross-sectional area (m^2)
A_{bit}	Cross-sectional area of drill bit (m^2)
C_l	Lift coefficient (-)
C_D	Drag coefficient (-)
C	Cuttings concentration (%)
CMC sol	Carboxymethyl cellulose solution
CTR	Cuttings Transport Ratio (-)
D_{pipe}	Drill pipe diameter (m)
D_{hole}	Hole diameter (m)
D	Diameter (m)
D_h	Hydraulic diameter (m)
d_s	Diameter of solids (m)
e	Eccentricity (-)
e_{ss}	Coefficient of restitution (-)

$\vec{F}_{lift,q}$	Lift force (N)
$\vec{F}_q$	External body force (N)
$\vec{F}_{wl,q}$	Wall lubrication force (N)
$\vec{F}_{d,q}$	Turbulent dispersion force (N)
$\vec{F}_{vm,q}$	Virtual mass force (N)
g	Gravitational acceleration ($m.s^{-2}$)
$g_{0,ss}$	Compressibility transition function (-)
I_{2D}	Second variant of the deviatoric stress (-)
$\vec{K}_{pq}$	Interphase momentum exchange coefficient (-)
K	Consistency index ($Pa.s^n$)
L_e	Entrance length (m)
$\dot{m}_{pq}$	Mass transfer from phase p to phase q ($kg.s^{-1}$)
$\dot{m}_{qp}$	Mass transfer from phase q to phase p ($kg.s^{-1}$)
n	Flow behaviour index (-)
p_s	Solids pressure (Pa)
q	Primary phase (-)
p	Secondary phase (-)
Re_t	Tube Reynolds number (-)
ROP	Rate of Penetration ($fthr^{-1}$)
$\vec{R}_{pq}$	Phase interaction force (N)
Re_p	Solid particles Reynolds number (-)
Re_ω	Vorticity Reynolds number (-)
Re_s	Relative Reynolds number (-)
S_q	Source term (-)
u_m	Mean flow velocity ($m.s^{-1}$)
$\vec{v}_{pq}$	Interphase velocity ($m.s^{-1}$)
$\vec{v}_q$	Primary phase velocity ($m.s^{-1}$)
$\vec{v}_p$	Secondary phase velocity ($m.s^{-1}$)
V_{cut}	Cuttings velocity ($m.s^{-1}$)

Greek letters

α_s	Solid phase volume fraction (-)
α_p	Secondary phase volume fraction (-)
$\mu_{s,\,col}$	Collisional viscosity (Pa.s)
$\mu_{s,\,kin}$	Kinetic viscosity (Pa.s)
$\mu_{s,\,fr}$	Frictional viscosity (Pa.s)
λ_s	Bulk viscosity (Pa.s)
λ_q	Primary phase bulk viscosity (Pa.s)
μ_f	Fluid viscosity (Pa.s)
μ_q	Primary phase viscosity (Pa.s)
Θ_s	Granular temperature (K)
ρ_s	Solid phase density ($kg.m^{-3}$)
ρ_q	Primary phase density ($kg.m^{-3}$)
ρ_f	Fluid density ($kg.m^{-3}$)
$\hat{\rho}_q$	Effective phase density ($kg.m^{-3}$)
β	Hole inclination angle (degrees)
φ	Cuttings bed porosity (%)
δ	Offset distance (m)
ϕ	Angle of internal friction (degrees)
α_l	Fluid phase volume fraction (-)

α_s	Solid phase volume fraction (-)
τ	Shear stress ($N.m^{-2}$)
$\bar{\bar{\tau}}_p$	p^{th} Phase stress-strain tensor (-)
γ	Shear rate (s^{-1})

8. Literature References

Al-Kayiem, H. H., Zaki, N. M., Asyraf, M. Z., & Elfeel, M. E., 2010. Simulation of the cuttings cleaning during the drilling operation. *Am. J. Appl. Sci.* **7**(6), 800–806.

Ataíde, C. H., Pereira, F. A. R., & Barrozo, M. A. S., 2007. CFD predictions of drilling fluid velocity and pressure profiles in laminar helical flow. *Braz. J. Chem. Eng.* **24**(4), 587–595.

Bilgesu, H. I., Ali, M. W., Aminian, K., & Ameri, S., 2002. Computational Fluid Dynamics (CFD) as a tool to study cutting transport in wellbores. In *SPE Eastern Regional Meeting*. Society of Petroleum Engineers.

Bilgesu, H., Mishra, N., & Ameri, S., 2007. Understanding the effect of drilling parameters on hole cleaning in horizontal and deviated wellbores using computational fluid dynamics. *Eastern Regional Meeting*. Society of Petroleum Engineers.

Capo, J., Yu, M., Miska, S., & Takach, N., 2004. Cuttings transport with aqueous foam at intermediate inclined wells. *SPE/ICoTA Coiled Tubing Conference and Exhibition.* Society of Petroleum Engineers.

Chen, Z., Ahmed, R., Miska, S., & Takach, N., 2007. Experimental study on cuttings transport with foam under simulated horizontal downhole conditions. *SPE Drill. & Compl.* **22**(04), 304-312.

Demiralp, Y., 2014. Effects Of Drill-pipe Whirling Motion on Cuttings Transport Performance for Horizontal Drilling. *Master dissertation*. Louisiana State University, USA.

Duan, M., Miska, S. Z., Yu, M., Takach, N. E., Ahmed, R. M., & Zettner, C. M., 2006. Transport of small cuttings in extended reach drilling. *International Oil & Gas Conference and Exhibition in China*. Society of Petroleum Engineers.

Duan, M., Miska, S., Yu, M., & Takach, N., 2010. Experimental study and modeling of cuttings transport using foam with drill pipe rotation. *SPE Drill. & Compl.* **25**(03), 352-362.

Eesa, M., & Barigou, M., 2009. CFD investigation of the pipe transport of coarse solids in laminar power law fluids. *Chem. Eng. Sci.* **64**(2), 322-333.

Fluent, A. (2017). 18.0 ANSYS Fluent theory guide 18.0. *Ansys Inc*, U.S.A.

Garcia-Hernandez, A. J., Miska, S. Z., Yu, M., Takach, N. E., & Zettner, C. M., 2007. Determination of cuttings lag in horizontal and deviated wells. *SPE Annual Technical Conference and Exhibition*. Society of Petroleum Engineers.

Gidaspow, D., 1994. Multiphase flow and fluidization: continuum and kinetic theory descriptions. Academic press.

Guckes, T., 1975. Laminar flow of non-Newtonian fluids in an eccentric annulus. *J. Eng. Ind.* **97**(2), 498-506.

Hajidavalloo, E., & Sadeghi-Behbahani-Zadeh, M., 2013. Simulation of gas–solid two-phase flow in the annulus of drilling well. *Chem. Eng. Res. Des.* **91**(3), 477-484.

Han, S., Hwang, Y., Woo, N., & Kim, Y., 2010. Solid–liquid hydrodynamics in a slim hole drilling annulus. *J. Pet. Sci. Eng.* **70**(3), 308-319.

Larsen, T., Pilehvari, A., & Azar, J., 1997. Development of a new cuttings-transport model for high-angle wellbores including horizontal wells. *SPE Drill. & Compl.* **12**(02), 129-136.

Li, Y., & Kuru, E., 2003. Numerical modelling of cuttings transport with foam in horizontal wells. *J. Can. Pet. Technol.* **42**(10).

Liu, Y., 2014. Two-fluid modeling of gas-solid and gas-liquid flows: solver development and application. *Doctoral dissertation*, Universitätsbibliothek der TU München.

Lun, C., Savage, S., & Jeffrey, D., 1984. Kinetic theories for granular flow: inelastic particles in Couette flow and slightly inelastic particles in a general flowfield. *J. Fluid Mech*. **140**, 223-256.

Mei, R., & Klausner, J. (1994). Shear lift force on spherical bubbles. *Int. J. Heat Fluid Flow* **15**(1), 62-65.

Mishra, N., 2007. Investigation of hole cleaning parameters using computational fluid dynamics in horizontal and deviated wells. *Master dissertation,* West Virginia University, USA.

Moraga, F., Bonetto, F., & Lahey, R., 1999. Lateral forces on spheres in turbulent uniform shear flow. *Int. J. Multiphase Flow.* **25**(6), 1321-1372.

Nguyen, D., & Rahman, S., 1996. A three-layer hydraulic program for effective cuttings transport and hole cleaning in highly deviated and horizontal wells. *SPE/IADC Asia Pacific Drilling Technology*. Society of Petroleum Engineers.

Ofei, T., Irawan, S., & Pao, W., 2014. CFD method for predicting annular pressure losses and cuttings concentration in eccentric horizontal wells. *J. Pet. Eng.*

Osgouei, R., 2010. Determination of cuttings transport properties of gasified drilling fluids. *Doctoral dissertation*, Middle East Technical University, Turkey.

Osunde, O., & Kuru, E., 2006. Numerical modelling of cuttings transport with foam in inclined wells. *Canadian International Petroleum Conference.* Petroleum Society of Canada

Ozbayoglu, M., Miska, S., Reed, T., & Takach, N., 2005. Using foam in horizontal well drilling: A cuttings transport modeling approach. *J. Pet.Sci.* **46**(4), 267-282.

Ozbayoglu, M. E., Saasen, A., Sorgun, M., & Svanes, K., 2010. Critical fluid velocities for removing cuttings bed inside horizontal and deviated wells. *Pet. Sci. Technol.* **28**(6), 594-602.

Pereira, F. A. R., Barrozo, M. A. S., & Ataíde, C. H., 2007. CFD predictions of drilling fluid velocity and pressure profiles in laminar helical flow. *Braz. J. Chem. Eng.* **24**(4), 587-595.

Pereira, F. A. R., Ataíde, C. H., & Barrozo, M. A. S., 2010. CFD approach using a discrete phase model for annular flow analysis. *Latin Am. Appl. Res.* **40**(1), 53–60.

Qutob, H., Mahli, Z., & Khlaifat, A., 2011. Enhancing ultimate recovery and adding reserves by underbalanced drilling technology. *SPE/IADC Middle East Drilling.* Society of Petroleum Engineers.

Roco, M. C., & Shook, C. A., 1983. Modeling of slurry flow: the effect of particle size. *Can. J. Chem. Eng.* **61**(4), 494–503.

Rooki, R., Ardejani, F., & Moradzadeh, A., 2015. CFD Simulation of Rheological Model Effect on Cuttings Transport. *J. Dispersion Sci. Tech.* **36**(3), 402-410.

Rooki, R., Doulati Ardejani, F., Moradzadeh, A., & Norouzi, M., 2014. Simulation of cuttings transport with foam in deviated wellbores using computational fluid dynamics. *J. Pet. Explor. Prod. Technol.* **4**(3), 263–273.

Saffman, P., 1965. The lift on a small sphere in a slow shear flow. *J.Fluid Mech.* **22**(02), 385-400.

Schaeffer, D., 1987. Instability in the evolution equations describing incompressible granular flow. *J. Diff. Eqns.* **66**(1), 19-50.

Shah, M. T., Utikar, R. P., Pareek, V. K., Tade, M. O., & Evans, G. M., 2015. Effect of closure models on Eulerian–Eulerian gas–solid flow predictions in riser. *Powder Technol.* **269**, 247-258.

Sorgun, M., 2010. Modeling of Newtonian fluids and cuttings transport analysis in high inclination wellbores with pipe rotation. *Doctoral Dissertation*. Middle East Technical Univeristy, Turkey.

Subramaniam, S., 2013. Lagrangian–Eulerian methods for multiphase flows. *Prog. Energy Combust. Sci.* **39**(2), 215-245.

Tomren, P., Iyoho, A., & Azar, J., 1986. Experimental study of cuttings transport in directional wells. *SPE Drill. Eng.* **1**(01), 43-56.

Wang, Z., Guo, X., Ming, L., & Hong, Y., 2009. Effect of drill pipe rotation on borehole cleaning for extended reach well. *J. Hydrodyn. Ser. B*. **21**(3), 366-372.

Wen, C. Y., & Yu, Y. H., 1966. Mechanics of fluidization. *Chem. Eng. Prog. Symp. Ser.* **62**(1), 100–111.

Yilmaz, D., 2012. Discrete Phase Simulations of Drilled Cuttings Transport Process in Highly Deviated Wells. *Master dissertation*, Louisiana State University, USA.

Zaisha, M., Chao, Y., & Kelessidis, V., 2012. Modeling and numerical simulation of yield viscoplastic fluid flow in concentric and eccentric annuli. *Chin. J. Chem. Eng*. **20**(1), 191-202.